Proc. Natl. Acad. Sci., India, Sect. A Phys. Sci. (April–June 2023) 93(2):401–412
https://doi.org/10.1007/s40010-023-00810-6

SCIENTIFIC RESEARCH PAPER

On the Structure of a Viscous Shock-Front in a Two-Phase Gas–Particle Medium

R. K. Anand[1] · **Anmol Singh**[1]

Received: 9 July 2022 / Revised: 18 September 2022 / Accepted: 6 January 2023 / Published online: 21 January 2023

Abstract The structure of the plane viscous shock-front in a two-phase gas–solid particle medium is investigated with the help of Navier–Stokes relation using the method of wave-front analysis. The analytical expressions for physical flow variables, i.e. the particle velocity, temperature, pressure, and change-in-entropy within the shock transition region have been derived taking into consideration the two-phase flow gas model. The influence on the structure of the shock-front due to the variation of different flow parameters such as coefficient of viscosity, Mach number, dust loading parameter, and the mass concentration of solid particles in the mixture is analysed. The thickness of the shock-front is calculated with varying different dust flow parameters within the shock transition region. In addition, variations in the thickness due to the viscosity and the shock strength have been observed. The results are compared with the case of dust-free medium. Interestingly, our findings confirm that flow parameters have a reasonable impact on the structure of a steady shock-front.

Keywords Two-phase flow · Shock-front thickness · Viscosity · Dust loading parameters

✉ R. K. Anand
anand.rajkumar@rediffmail.com; rkanand@allduniv.ac.in

Anmol Singh
anmolsingh2018@gmail.com

[1] Department of Physics, UGC Centre of Advanced Studied, University of Allahabad, Prayagraj 211002, India

1 Introduction

The non-availability of an ideal gas compared to dusty gaseous medium, the problem of shock waves propagating in different media such as astronomical and geophysical have attracted much attention by the researchers. With this consideration, several authors [1–6] have studied taking into account various aspects such as structure, two-phase, multiphase flow [7, 8] and effect of solid dust particles on its propagation. Carrier [9] presented the first theoretical study of shock wave propagation in dusty gaseous mixtures with solid particles. Rudinger [10] has shown that solid particles have a significant effect on the structure of shock waves. Ben-Dor [11] did an improved version of his previous work [see Ref. 6] by addition of new assumptions such as attenuation and validation of the shock governing equations during propagation in two-phase flow medium.

A more generalized study on the shock wave structure in a mixture of gas–solid particles was done by Pai et al. [12, 13]. Different techniques and methods have been applied to better understand the shock wave problems such as blast waves [14, 15], piston problem [16, 17] and shock tube problem [18]. In addition, several research works have been reported under different physical conditions like interactions of shock waves in different media [19], and jump conditions [20] across the shock. Much work has been done by the researchers on the shock waves propagation using various techniques [21–23].

Hamad [24, 25] derived an analytical solution for the structure of shock-front and obtained its thickness due to the various flow variables in a two-phase flow medium, which is a mixture of solid dust particles in a gas. The thickness of the shock-front, which is equal to the order of mean free path of the gas particles, mainly depends on the Mach number that characterizes the strength of shockwave. Our

current study is also focused to determine the thickness of a steady shock-front. Previously, various methods have been developed for finding the thickness of the shock-front. Robben et al. [26] found the thickness of the shock-front using the method of electron beam techniques. Elizarova et al. [27] obtained the thickness of shock-front at different Mach numbers for various gases using Navier–Stokes (NS) and quasi-gasdynamics (QGD) equations. These results are in good agreement with theoretical studies. The variation of total enthalpy was numerically investigated in monatomic gases using Monte Carlo approach by Shoev et al. [28] Recently, Bisi et al. [29] obtained the thickness of shock-front for binary gas mixture using BKG hydrodynamic description limitations. The authors have calculated the shock-front thickness in a monatomic gaseous media within the shock transition region using different flow variables that characterize the thickness of stationary shock-front. Subsequently, they have also calculated the thickness of the binary gas mixture.

A new scaling is developed for the simulation and shock wave structure in both air and underwater blast waves based on dimensional analysis [30, 31]. Elizarova [32] obtained the numerical simulation of one-dimensional stationary shock-front thickness using Navier–Stokes equations of Nitrogen gas. Enhancement of shock capturing methods via machine learning [33] has been proposed for the scaling of the shock-waves structure.

In the two-phase flow, mixture of gas and solid dust particles, the study of shock wave has more significance due to its wide applications in the field of geophysical, astrophysical, aerospace engineering and medical sciences [34–38]. Recent development in the field of shock waves encompasses areas such as plasma physics [39, 40], nanofluids [41], laser shock waves [42], and shock in metals [43, 44] in order to evaluate enhancement, stagnation and stability of shocks. Anand and Yadav [45] have investigated the effects of viscosity on the structure of shock waves in a real gaseous medium.

In the present work, we have explored the internal structure of the viscous shock-front in a medium consisting of gas–solid particles. Non-dimensional analytical expressions of different flow variables such as the particle velocity, temperature, pressure and change-in-entropy distribution have been obtained within the shock transition region. With the help of various flow parameters, including dust loading parameters, the variations in the flow variables are obtained analytically and are shown graphically. We have also discussed the variation in the thickness of the shock-front with flow parameters. The obtained results are compared with the thickness of the shock-front in dust-free medium. Interestingly, our present analysis shows that flow parameters have a reasonable impact on the structure of the shock-front. For these studies MATLAB code is used to make numerical computations and to plot graphs.

2 Basic Equations of Motion and Boundary Conditions

The conservation equations governing the motion of a one-dimensional, unsteady, planar and viscous flow in a dusty gas in equilibrium condition can be written in Eulerian coordinates as follows:

$$\frac{\partial \rho}{\partial t} + \rho \frac{\partial u}{\partial r} + u \frac{\partial \rho}{\partial r} = 0 \tag{1}$$

$$\frac{\partial (\rho u)}{\partial t} + \frac{\partial (p + \rho u^2 - q)}{\partial r} = 0 \tag{2}$$

$$\frac{\partial (\rho e + \rho u^2 / 2)}{\partial t} + \frac{\partial [\rho u (e + u^2 / 2) + pu - qu]}{\partial r} = 0 \tag{3}$$

where $\rho(r,t)$, $u(r,t)$ and $p(r,t)$ are the fluid density, fluid velocity and pressure of the mixture, respectively. Also, $e(r,t)$ is the internal energy of the mixture per unit mass, $q(r,t)$ is the viscous stress tensor, r is the space coordinate measured in the direction normal to the shock-front from the origin O, and, t is the time coordinate with respect to shock-front.

The expression for the equation of state for a mixture of perfect gas and small solid particles [13] is given by

$$p = \frac{(1 - k_p)\rho R_i T}{(1 - Z)} \tag{4}$$

where $k_p (k_p = m_{\mathrm{sp}} / m)$ is the mass concentration of solid particles (m_{sp}) in the mixture (m), Z is the volumetric fraction of solid particles in the mixture, R_i and T are the gas constant and absolute temperature of the mixture, respectively.

The relation between k_p and Z is given by [12]

$$k_p = \frac{Z \rho_{\mathrm{sp}}}{\rho} \tag{5}$$

where $Z = \frac{Z_0 \rho}{\rho_0}$, while ρ_{sp} is the species density of the solid particles. The subscript '0' refers to the initial values of Z and ρ. It should be mentioned at this point, in our present work we have taken the value of Z in the range $0.05 < Z < 0.1$. This is because for lower value of $Z (Z < 0.05)$, the volume fraction of the particles in the mixture is negligibly small. Since, for equilibrium flow, k_p is a constant quantity in the whole flow field, consequently, Z/ρ is also a constant. Note that $k_p = 0$ corresponds to the case of dust-free medium.

In general, the initial volume fraction Z_0 is not a constant, however, the volume occupied by the solid particles is very small ($\sim 10^{-3}\mathrm{m}^3$) as the density of the solid particles is much larger than that of the gas. Hence, Z_0 may be assumed to be a constant. Thus, we can write Z_0 in terms of k_p and G in the following form, [12]

$$Z_0 = \frac{k_p}{G(1-k_p)+k_p}, \tag{6}$$

where G refers to a dust laden parameter which is the ratio of the density of solid particles to the initial density of perfect gas in the mixture.

The internal energy of the mixture is given by,

$$e = \left[k_p C_{\mathrm{sp}} + (1-k_p)C_v\right]T = C_{vm}T, \tag{7}$$

where C_{sp} is the specific heat of the solid particles, C_{vm} and C_v are the specific heats of the mixture and the gas at constant volume, respectively.

The ratio of specific heats at constant pressure (C_{pm}) and volume (C_{vm}) of the mixture is expressed as [6, 12]

$$\Gamma = \frac{C_{pm}}{C_{vm}} = \frac{\gamma + \delta\beta}{1+\delta\beta}, \tag{8}$$

where $\gamma = \frac{C_p}{C_v}$, $\beta = C_{sp}/C_v$, and $\delta = \frac{k_p}{(1-k_p)}$.

Thus, the internal energy per unit mass of the mixture becomes

$$e = \frac{(1-Z)p}{(\Gamma-1)\rho}. \tag{9}$$

The viscous stress tensor (q) in terms of the coefficient of viscosity is given by,

$$q = \frac{4}{3}\mu\frac{\mathrm{d}u}{\mathrm{d}r} \tag{10}$$

where μ is the coefficient of viscosity. In order to obtain the structure of the shock-front, we consider a coordinate system in which the shock-front is at rest within a small-time interval. We assume that, in this small-time interval, the order of the shock-front thickness does not change. It is customary in hydrodynamics to discard terms containing partial time derivatives $\left(\frac{\partial}{\partial t}\right)$ in Eqs. (1–3). Also, the partial derivative $(\partial/\partial r)$ with respect to distance is replaced by a total derivative $\left(\frac{d}{dr}\right)$. With this consideration, Eqs. (1–3) becomes,

$$u\frac{\mathrm{d}\rho}{\mathrm{d}r} + \rho\frac{\mathrm{d}u}{\mathrm{d}r} = 0 \tag{11}$$

$$\frac{\mathrm{d}(p+\rho u^2 - q)}{\mathrm{d}r} = 0 \tag{12}$$

$$\frac{\mathrm{d}[\rho u(e+u^2/2) + pu - qu]}{\mathrm{d}r} = 0. \tag{13}$$

To obtain the solutions of Eqs. (11–13) we shall use the boundary conditions which require that the gradient of the flow variables must vanish for $r \to \pm\infty$ in the shock-front region. In the discussion that follows, we use certain usual notations such as p_0, ρ_0, u_0 and p, ρ, u to signify the value of flow variables just ahead and behind the shock-front region, respectively. We also assume that the moving velocity of the shock-front is U, and, therefore, for the coordinate system fixed with the shock-front, the initial particle velocity is,

$$u_0 = U. \tag{14}$$

We shall now obtain and then discuss the analytical solution for the flow variables in the next section.

3 Exact Solutions for the Flow Variables

In order to obtain the analytical expressions for the flow variables, we solve Eqs. (11)–(13) with the help of boundary condition specified by Eq. (14), and use Eq. (9) to obtain the system of equations as

$$\rho = \rho_0 U/u \tag{15}$$

$$p = p_0 + q + \rho_0 U^2 - \rho u^2 \tag{16}$$

$$\begin{aligned} &pu(\Gamma - Z) + (\Gamma-1)\frac{\rho u^3}{2} - qu(\Gamma-1) \\ &= p_0 U(\Gamma - Z_0) + \frac{\rho U^3}{2}(\Gamma-1). \end{aligned} \tag{17}$$

Using Eqs. (15–16), we write Eq. (17) as,

$$\begin{aligned} &(p_0 + \rho_0 U^2)(\Gamma - Z)u - \frac{\rho u^3}{2}(1+\Gamma-2Z) \\ &+ q(1-Z)u = p_0 U(\Gamma - Z_0) + \frac{\rho_0 U^3}{2}(\Gamma-1) \end{aligned} \tag{18}$$

To obtain the flow variables in non-dimensional terms which give the characteristics scale, we introduce following two non-dimensional parameters called particle velocity η and shock strength M as,

$$\eta = u/U = \rho_0/\rho, \quad Z = \frac{Z_0\rho}{\rho_0} = \frac{Z_0}{\eta}$$

with

$$M = U/a_0 \tag{19}$$

where the parameter $a_0^2 = \left(\frac{\Gamma\delta_0 p_0}{\rho_0}\right)$ represents the speed of sound in the unperturbed medium with $\delta_0 = 1/(1 - Z_0)$.

With the help of Eqs. (9, 10, 15 and 19), Eq. (18) becomes

$$A\eta^2 + B\eta + C = g(\eta - Z_0)\frac{d\eta}{dr}. \tag{20}$$

Here, $A = (\Gamma + 1)/2$, $B = -\left(1/\delta_0 M^2 + \Gamma + Z_0\right)$, $C = \left(Z_0 + 1/\delta_0 M^2 + (\Gamma - 1)/2\right)$, and $g = \frac{4\mu}{3M\left(\Gamma\delta_0 p_0 \rho_0\right)^{1/2}}$.

Since, Eq. (20) is quadratic in η, and in equilibrium state the gradient of flow variables vanishes, therefore, $\mathrm{d}\eta/\mathrm{d}r = 0$ with $\eta = \eta_{eq}$.

For η_{eq} the two solutions of Eq. (20) are,

$$\eta_{eq} = \left[-B \pm \sqrt{B^2 - 4AC}\right] \Big/ 2A.$$

We denote the equilibrium states η_1 and η_2 with positive and negative sign, respectively, as,

$$\eta_{1,2} = \left[-B \pm \sqrt{B^2 - 4AC}\right] \Big/ 2A \tag{21}$$

Integrating Eq. (20) and using Eq. (21), we get an expression of the flow variables in terms of the particle velocity,

$$r = (g/A)\left[X \log\left(\eta - \eta_1\right) + Y \log\left(\eta - \eta_2\right)\right] + C' \tag{22}$$

where C' is a constant of integration.

To obtain the value of C', we choose the origin O of coordinate system at a point where the slope $(\mathrm{d}\eta/\mathrm{d}r)$ of the particle velocity becomes maximum. This maxima occurs at the point of inflection which is given by the condition $\mathrm{d}^2\eta/\mathrm{d}r^2 = 0$. On using this condition in Eq. (20), we get

$$\mathrm{d}^2\eta/\mathrm{d}r^2 = A\eta^2 - 2A\eta Z_0 - (C + BZ_0) = 0. \tag{23}$$

In all the possible roots extracted from Eq. (23), consider that $\eta = \eta'_{eq}$ is the maximum value of the real root at the origin (r=0) in the flow field region, which satisfies the equation completely. So, the solution of Eq. (23) which enables us to obtain the point of inflection is

$$\eta'_{eq} = Z_0 \pm \sqrt{\{(Z_0)^2 + (C + BZ_0)/A} \tag{24}$$

Using this condition, we get the constant of integration C' from Eq. (22) as

$$C' = -(g/A)\left[X \log\left(\eta'_{eq} - \eta_1\right) + Y \log\left(\eta'_{eq} - \eta_2\right)\right] \tag{25}$$

Substituting the value of C' from Eq. (25) into Eq. (22), we get the exact solution for the particle velocity with respect to position as

$$\begin{aligned} r = (g/A)\Big[&\alpha \log\left\{\left(\eta - \eta_1\right)\Big/\left(\eta'_{eq} - \eta_1\right)\right\} \\ &+\beta \log\left\{\left(\eta - \eta_2\right)\Big/\left(\eta'_{eq} - \eta_2\right)\right\}\Big] \end{aligned} \tag{26}$$

where $\alpha = (\eta_1 - Z_0)/(\eta_1 - \eta_2)$ and $\beta = (\eta_2 - Z_0)/(\eta_2 - \eta_1)$.

To obtain the exact solution for the temperature distribution within the shock transition region, we use Eqs. (7, 9, 10 and 17) to obtained,

$$\begin{aligned} T/T_0 =& 1 + \Gamma\delta_0^2 M^2(\Gamma - 1) \\ &\left[\eta^2/2 - \left(1 + 1/\Gamma\delta_0 M^2\right)\eta\right. \\ &\left.+\left(1/2 + 1/\Gamma\delta_0 M^2\right)\right] \end{aligned} \tag{27}$$

Equation (27) correlates the temperature and the particle velocity in a two-phase gas-particle flow medium. Using relations given by Eqs. (26) and (27), we can compute the temperature distribution within the shock transition region with respect to position.

Similarly, by using Eqs. (10, 15, 20 and 16) we can obtain the exact solution for the pressure distribution within the shock transition region as,

$$p/p_0 = 1 + \Gamma\delta_0 M^2\left[(1 - \eta) + (A\eta^2 + B\eta + C)/(\eta - Z_0)\right] \tag{28}$$

Equations (26) and (28) together describe the pressure distribution across the shock-front region with respect to space coordinates. In addition, with the help of Eq. (28), we can also obtain the change-in-entropy across the shock-front of arbitrary strength in a dusty gaseous medium as,

$$\begin{aligned} \Delta S/R_i =& \left((1 - k_p)/(\Gamma - 1)\right) \\ &\left[log\left(p/p_0\right) - \Gamma \log(1/\eta)\right. \\ &\left.+\Gamma \log\left(1 - Z_0/\eta\right)/(1 - Z_0)\right] \end{aligned} \tag{29}$$

The variations in the flow variables $(\eta,\ T/T_0,\ p/p_0\ , \Delta s/R_i)$ are shown in Figs. 1, 2, 3 and 4 within the shock-front in a dusty gaseous medium.

4 Results and Discussion

The non-dimensional exact solutions for the flow variables such as $\eta,\ T/T_0,\ p/p_0$ *and* $\Delta s/R_i$ corresponding to the particle velocity, temperature, pressure, and the change-in-entropy within the shock transition region and are given by Eqs. (26–29), respectively. Here, in order to obtain an exact analytical solution to the flow variables, we have neglected the overtaking disturbances due to the reflections, wave interactions in wake, gravitational effects, etc. in the flow field region of the shock wave-front.

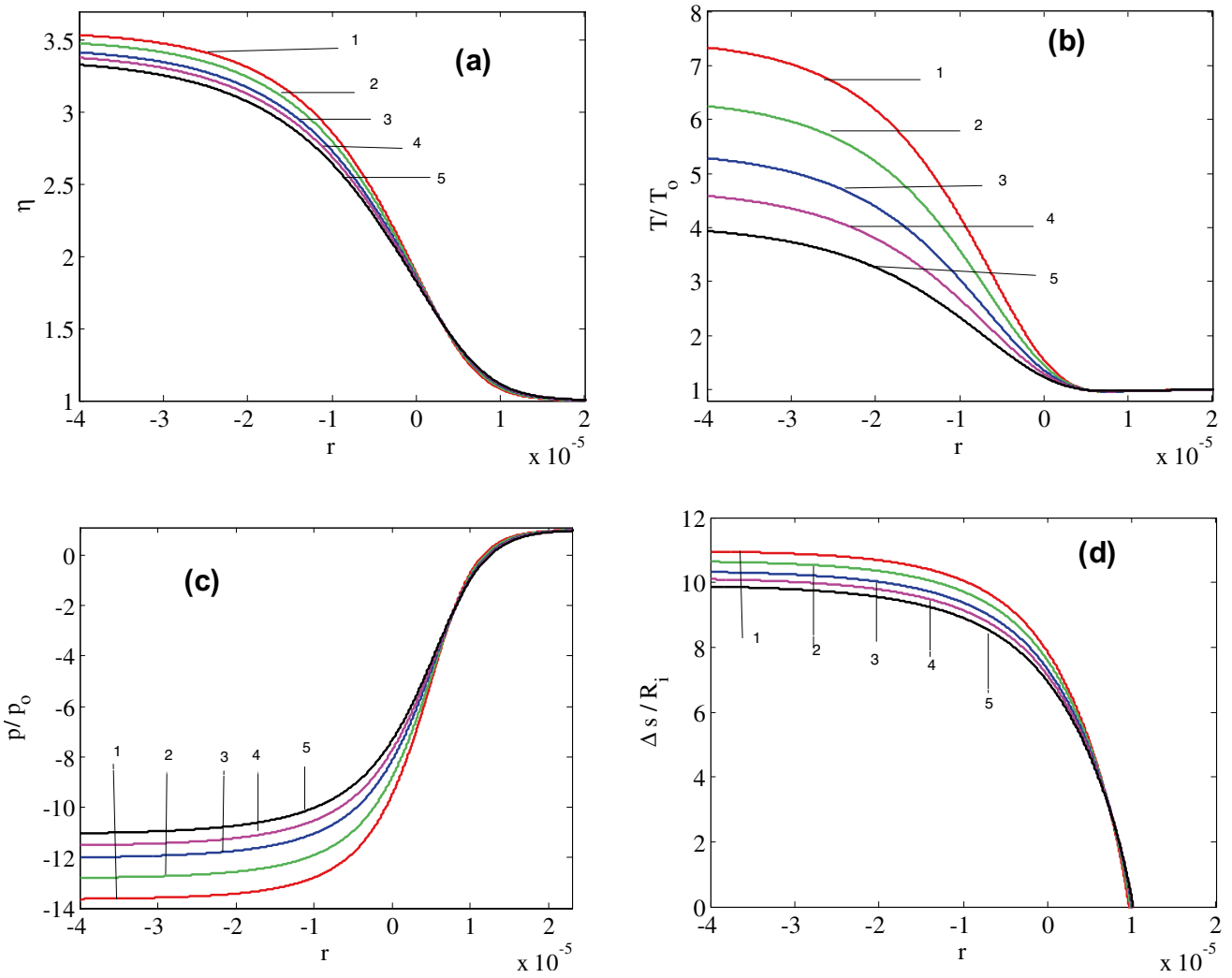

Fig. 1 Variations of non-dimensional flow variables: **a** particle velocity (η), **b** temperature (T/T_0), **c** pressure (p/p_0), and **d** change-in-entropy ($\Delta s/R_i$), within the shock transition region for $M=2$, $\mu = 15.0 \times 10^{-6}$ Pa s, $\gamma = 1.4$, $\beta = 1$, $p_0 = 0.9$ bar, and $\rho_0 = 1.20$kg m^3. Here, different curves corresponds to 1. $k_p = 0$ Dust-free case) 2. $k_p = 0.1$, $G=10$, 3. $k_p = 0.2$, $G=10$, 4. $k_p = 0.3$, $G=10$, 5. $k_p = 0.4$, $G=10$

The analytical expressions for the flow variables are the functions of the position, Mach number (M), coefficient of viscosity μ, adiabatic exponent γ, mass concentration in the mixture k_p, and dust laden parameter G of the two-phase gas-particle mixture. For numerical computations, we have assigned the values to the parameters as $M = \{1.1,\ 1.5,\ 2.0\}$, $\gamma = 1.4$, $\beta = 1$, $k_p = \{0,\ 0.1,\ 0.2,\ 0.3,\ 0.4\}$, $\mu = \{15,\ 17.5,\ 20\} \times 10^{-6}$ Pa s, and dust loading parameter $G = \{1,\ 10,\ 100,\ 1000\}$, along with initial pressure $p_0 = 0.9$ bar, initial density $\rho_0 = 1.20$ kg m^3. The value of $k_p = 0$ will lead to the case of a perfect gas. The effect of dust particles on the flow variables within the shock transition region is depicted in Figs. 1, 2, 3 and 4. Here, we have used MATLAB code to plot the graphs for the flow variables.

Following inferences can be drawn by observing Table 1:

1. **For the case of shock strength** (M):
2. At fixed value of $M = 1.1$, on increasing the value of k_p from 0 to 0.1, i.e. for perfect to dusty gaseous medium, the thickness of the shock-front decreases sharply. In addition, with increasing k_p in the range ($0.1 \le k_p \le 0.4$), the thickness of the shock-front decreases except for the case of $k_p = 0.3$, for which it increases. Similar variation has also been observed for each value of μ.
3. For $M = 1.5$, the thickness of shock-front increases on going from dust-free ($k_p = 0$) to dusty gaseous medium ($k_p = 0.1$) and also for higher value of k_p, i.e. for $k_p > 0.3$, whereas a decrement in the shock-front thickness is observed when k_p lies in the range ($0.1 \le k_p \le 0.3$).

Table 1 The thickness of the shock-front for different values of M, μ, k_p, Γ with $G = 10$, $\gamma = 1.4$, $\beta = 1$, $p_0 = 0.9$ bar, $\rho_0 = 1.20$ kg m^3

Coefficient of viscosity [Pa s]	M	k_p	Γ	r_1 [m]	r_2 [m]	$r_2 - r_1$ [m]
15×10^{-6}	1.1	0	1.40	− 0.0026450	0.0006903	0.0033353
		0.1	1.36	− 0.0010790	0.0006970	0.0017760
		0.2	1.32	− 0.0008336	0.0007029	0.0015365
		0.3	1.28	− 0.0011540	0.0007077	0.0018617
		0.4	1.24	− 0.0010170	0.0007107	0.0017277
	1.5	0	1.40	− 0.0002101	0.0001019	0.0003120
		0.1	1.36	− 0.0002459	0.0001029	0.0003488
		0.2	1.32	− 0.0002288	0.0001038	0.0003326
		0.3	1.28	− 0.0002136	0.0001046	0.0003182
		0.4	1.24	− 0.0002232	0.0000988	0.0003220
	2.0	0	1.40	− 0.0001167	0.0000330	0.0001497
		0.1	1.36	− 0.0001265	0.0000333	0.0001598
		0.2	1.32	− 0.0001231	0.0000355	0.0001586
		0.3	1.28	− 0.0001410	0.0000358	0.0001768
		0.4	1.24	− 0.0001533	0.0000340	0.0001873
17.5×10^{-6}	1.1	0	1.40	− 0.0030860	0.0008053	0.0038913
		0.1	1.36	− 0.0012590	0.0008131	0.0020721
		0.2	1.32	− 0.0009725	0.0008201	0.0017926
		0.3	1.28	− 0.0013470	0.0008257	0.0021727
		0.4	1.24	− 0.0011870	0.0008291	0.0020161
	1.5	0	1.40	− 0.0002451	0.0001189	0.0003640
		0.1	1.36	− 0.0002869	0.0001201	0.0004070
		0.2	1.32	− 0.0002670	0.0001140	0.0003810
		0.3	1.28	− 0.0002492	0.0001220	0.0003712
		0.4	1.24	− 0.0002605	0.0001225	0.0003830
	2.0	0	1.40	− 0.0001362	0.0004071	0.0001769
		0.1	1.36	− 0.0001476	0.0004112	0.0001887
		0.2	1.32	− 0.0001437	0.0004149	0.0001851
		0.3	1.28	− 0.0001645	0.0000395	0.0002040
		0.4	1.24	− 0.0001789	0.0000397	0.0002186
20×10^{-6}	1.1	0	1.40	− 0.0035270	0.0009204	0.0044474
		0.1	1.36	− 0.0014390	0.0009293	0.0023683
		0.2	1.32	− 0.0011110	0.0009372	0.0020482
		0.3	1.28	− 0.0015390	0.0009436	0.0024826
		0.4	1.24	− 0.0013560	0.0009476	0.0023036
	1.5	0	1.40	− 0.0002801	0.0001279	0.0004080
		0.1	1.36	− 0.0003278	0.0001372	0.0004650
		0.2	1.32	− 0.0003051	0.0001303	0.0004354
		0.3	1.28	− 0.0002848	0.0001394	0.0004242
		0.4	1.24	− 0.0002977	0.0001400	0.0004377
	2.0	0	1.40	− 0.0001556	0.0000465	0.0002021
		0.1	1.36	− 0.0001687	0.0000470	0.0002157
		0.2	1.32	− 0.0001642	0.0000474	0.0002116
		0.3	1.28	− 0.0001880	0.0000477	0.0002357
		0.4	1.24	− 0.0002044	0.0000454	0.0002498

4. For the case of $M=2$, the variation in the shock-front thickness is similar to the case of $M=1.5$. The thickness first increases on increasing the value of k_p from ideal ($k_p=0$) to dusty medium ($k_p\neq 0$). Subsequently, decrement is observed for the range $k_p=0.1$ to 0.2 and it again starts to increase for $k_p\geq 0.3$. The obtained results are the same for different values of μ.

Following conclusions can be drawn from the above observations for different values of M and k_p:

1. As we go from ideal to dusty gaseous medium by increasing k_p from 0 to 0.1, the structure of shock-front thickness increases except for the case of $M=1.1$, for which it decreases. This has an implication that for lower value of shock strengths ($M=1.1$), the collision between solid dust particles is considerably low compared to the

Table 2 The shock-front thickness for different values of k_p and G, for fixed $M=2$, $\mu=15\times10^{-6}$ Pa s, $\gamma=1.4$, $\beta=1$, $p_0=0.9$ bar, $\rho_0=1.20$ kg m^3

k_p	G	Γ	r_1 [m]	r_2 [m]	r_2-r_1 [m]
0.1	1	1.36	− 0.0001183	0.00003157	0.00014987
	10	1.32	− 0.0001265	0.00003335	0.00015985
	100	1.28	− 0.0001409	0.00003545	0.00017635
0.2	1	1.36	− 0.0001138	0.00003171	0.00014551
	10	1.32	− 0.0001231	0.00003556	0.00015866
	100	1.28	− 0.0001262	0.00003409	0.00016029
0.3	1	1.36	− 0.0001089	0.00002822	0.00013712
	10	1.32	− 0.0001410	0.00003390	0.00017490
	100	1.28	− 0.0001281	0.00003661	0.00016471

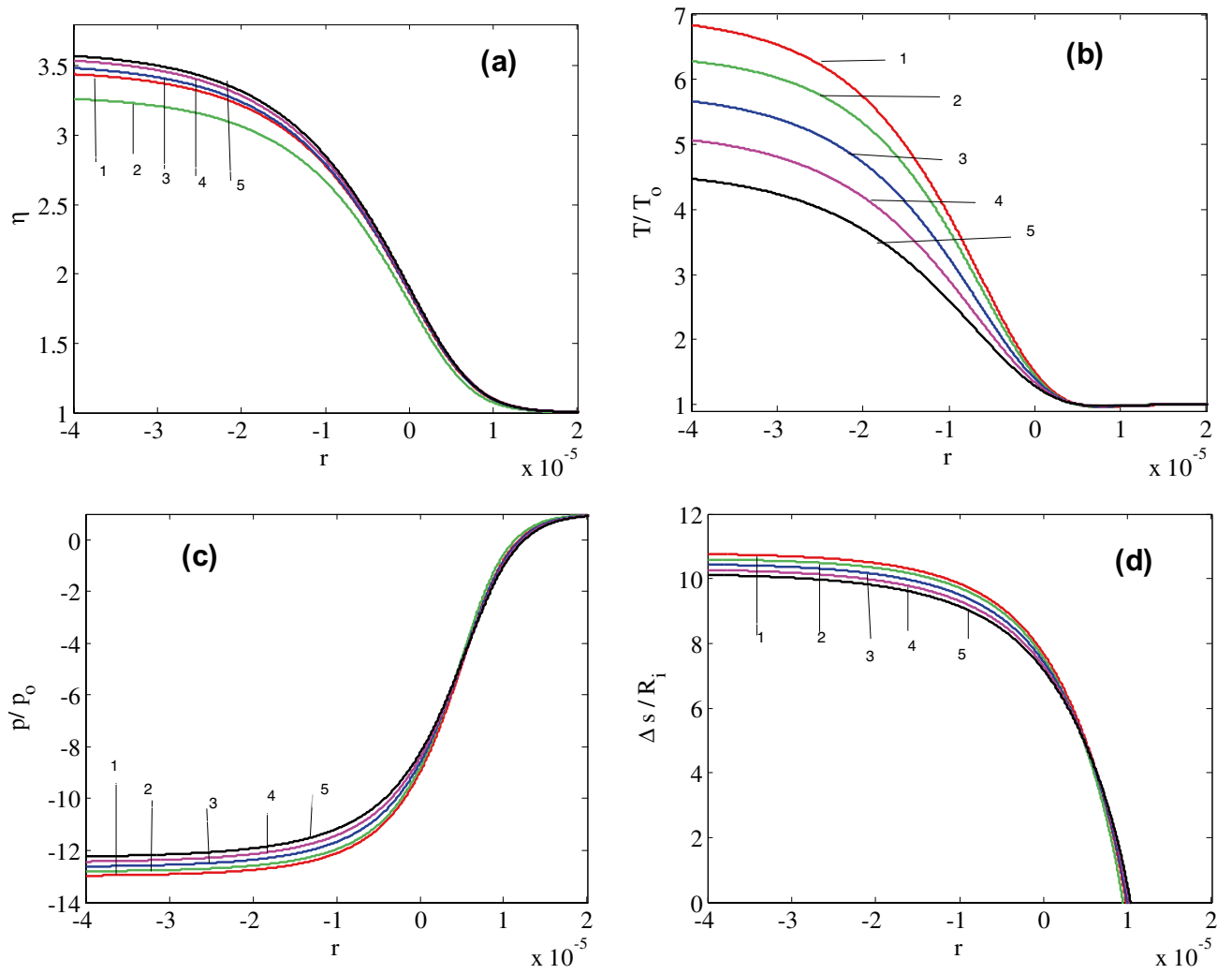

Fig. 2 Variations of non-dimensional flow variables: **a** the particle velocity (η), **b** temperature (T/T_0), **c** pressure (p/p_0), and **d** change-in-entropy ($\Delta s/R_i$) distribution within the shock transition region for, $M=2$, $\mu=15.0\times10^{-6}$ Pa s, $\gamma=1.4$, $\beta=1$, $p_0=0.9$ bar, and $\rho_0=1.20$ kg m^3. Here different curves stand for: 1. $k_p=0$ (Dust-free case) 2. $k_p=0.2$, $G=1$, 3. $k_p=0.2$, $G=10$, 4. $k_p=0.2$, $G=100$, 5. $k_p=0.2$, $G=1000$

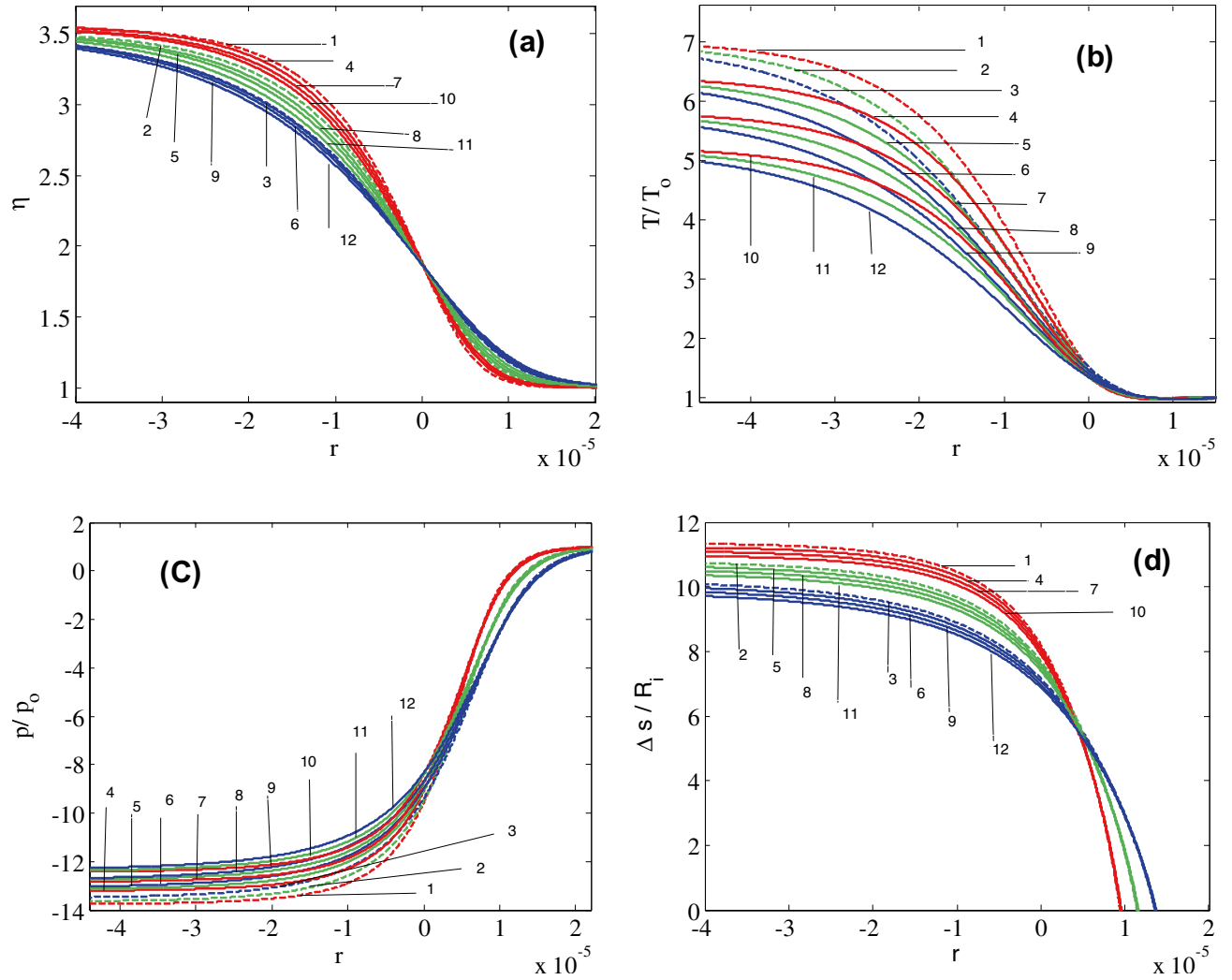

Fig. 3 Variations of non-dimensional flow variables: **a** the particle velocity (η), **b** the temperature (T/T_0), **c** the pressure (p/p_0), **d** the change-in-entropy ($\Delta s/R_i$) distribution within shock transition region in case of $M=2$, $\gamma = 1.4$, $G=10$, $\beta = 1$, $p_0 = 0.9$ bar, and $\rho_0 = 1.20$ kg m^3 Here, different curves stand for: 1. $k_p = 0$,(Dust-free case), $\mu = 15 \times 10^{-6}$ Pa s, 2. $k_p = 0$(Dust-free case), $\mu = 17.5 \times 10^{-6}$ Pa s, 3. $k_p = 0$(Dust-free case), $\mu = 20 \times 10^{-6}$ Pa s, 4. $k_p = 0.1$, $\mu = 15 \times 10^{-6}$ Pa s, 5. $k_p = 0.1$, $\mu = 17.5 \times 10^{-6}$ Pa s, 6. $k_p = 0.1$, $\mu = 20 \times 10^{-6}$ Pa s, 7. $k_p = 0.2$, $\mu = 15 \times 10^{-6}$ Pa s, 8. $k_p = 0.2$, $\mu = 17.5 \times 10^{-6}$ Pa s, 9. $k_p = 0.2$, $\mu = 20 \times 10^{-6}$ Pa s, 10.$k_p = 0.3$, $\mu = 15 \times 10^{-6}$ Pa s, 11.$k_p = 0.3$, $\mu = 17.5 \times 10^{-6}$ Pa s, 12.$k_p = 0.3$, $\mu = 20 \times 10^{-6}$ Pa s

case of high shock strength (e.g. $M=1.5$, 2.0). Hence, the thickness of the shock-front gives opposite behaviour for such values of k_p.

2. We also observe that with an increase in the mass concentration of solid particles in a dusty gaseous medium, which is a mixture of perfect gas and solid dust particles, k_p from 0 to 0.3, the thickness of shock-front begins to decrease in the case of $M=1.1$, whereas it increases in the cases of $M=1.5$, 2, onwards. This may be due to the low shock strength, even if the mass concentration of solid dust particles in the mixture k_p is increasing, due to fewer collisions of the particles with each other, so it does not have much impact on the structure of the shock-front. As a result, the pattern of the graph decreases sequentially. On the other hand, at higher values of shock strength, *i.e.* $M \geq 2$, the thickness begins to increase at $k_p = 0.2$ due to greater shock strength solid dust particles collide with each other more frequently. So, the thickness starts increasing from $k_p = 0.2$.

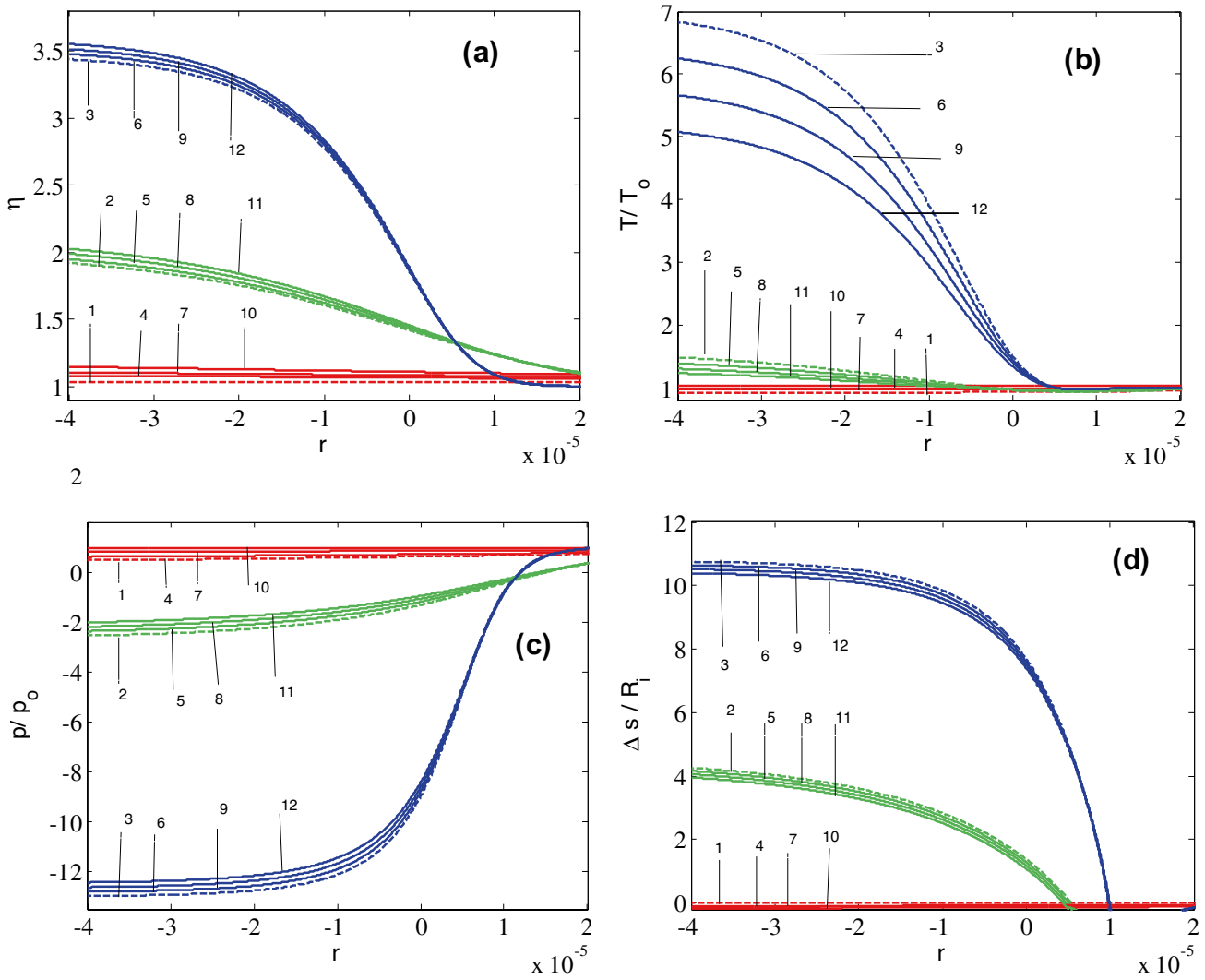

Fig. 4 Variations of non-dimensional flow variables: **a** the particle velocity (η), **b** the temperature (T/T_0), **c** the pressure (p/p_0), **d** entropy production ($\Delta s/R_i$) within the shock transition region for the case of $\mu = 15.0 \times 10^{-6}$ Pa s, $\gamma = 1.4$, $G = 10$, $\beta = 1$, $p_0 = 0.9$ bar, and $\rho_0 = 1.20$. $\rho_0 = 1.20$kg m^3. 1. $M = 1.1$, $k_p = 0$,(Dust-free case), 2. $M = 1.5$, $k_p = 0$(Dust-free case), 3. $M = 2.0$, $k_p = 0$(Dust-free case),4. $M = 1.1$, $k_p = 0.1$, 5. $M = 1.5$, $k_p = 0.1$, 6. $M = 2.0$, $k_p = 0.1$, 7. $M = 1.1$, $k_p = 0.2$, 8. $M = 1.5$, $k_p = 0.2$, 9. $M = 2.0$, $k_p = 0.2$, 10. $M = 1.1$, $k_p = 0.3$, 11. $M = 1.5$, $k_p = 0.3$, 12. $M = 2.0$, $k_p = 0.3$.

The above findings indicate that the shock strength (M) and solid dust particles in the mixture (k_p) are the major factors that govern the thickness of the shock-front.

5 For the case of coefficient of viscosity (μ)

1. As the value of μ increases, the thickness of shock-front increases in both dust-free case ($k_p = 0$) and dusty gaseous media ($k_p \neq 0$), and for all values of M.

Our results are in good agreement with that of Anand et al. [45] for the case of an ideal gas.

It can be observed from Table 2 that the shock-front thickness increases with increasing dust laden parameter G ($1 \leq G \leq 100$), and for fixed value of k_p. We also notice that with increasing k_p, and with constant G, the decrease in the thickness is small. Therefore, we may conclude that the dust laden parameter (G) plays a significant role in determining the thickness of shock-front.

The variations in the flow variables within the shock transition region with respect to position (r), and for different values of k_p are shown in Fig. 1. In these plots, we have chosen the flow parameters as, $M = 2$, $G = 10$, $\mu = 15.0 \times 10^{-6}$ Pa s, $\gamma = 1.4$, $\beta = 1$, $p_0 = 0.9$ bar, $\rho_0 = 1.20$ kg m^3. It is observed that the spreading in the flow variables such as the particle velocity (η), temperature (T/T_0), pressure (p/p_0), and

change-in-entropy distribution ($\Delta s/R_i$) decreases as we move from upstream to downstream. The separation between the curves, which is quite indistinguishable at the upstream, gradually increases to become distinct towards the downstream. The spreading of the flow variables is larger for $k_p = 0$ which decreases with increasing k_p. Thus, it can be concluded that the thickness of the shock-front increases as we increase the mass concentration of dusty particles in the medium.

The expressions as given in Eqs. (26–29) for the variations in the flow variables within the shock transition region with the distance r for different values of G, at a fixed value of $M=2$, $k_p = 0,\ 0.2$, $\mu = 15 \times 10^{-6}$ Pa s, $\gamma = 1.4$, $\beta = 1$, $p_0 = 0.9$ bar, $\rho_0 = 1.20$ kg m^3 are shown in Fig. 2. It can be seen from Fig. 2, that the spreading of the flow variables such as the particle velocity (η), temperature (T/T_0), pressure (p/p_0), and change-in-entropy ($\Delta s/R_i$) are distinguishable towards the downstream side, *i.e.* ahead of the point of inflection, whereas these plots are indistinguishable towards the upstream side. The spreading of flow variables is large at $k_p = 0$, $G=1$ and with increasing G, the spreading of the flow variables conserved and tends to be indistinguishable towards the upstream side. In addition, Fig. 2 shows that the spreading is large at $G=1$, and with increasing G, the spreading increases sharply. Thus, the thickness of shock-front increases with increasing dust laden parameter G. On comparing of Fig. 2 with Fig. 1, it is clear that the thickness obtained by changing G is less than the thickness obtained by changing k_p. This means that the thickness of the shock-front is less affected by G than by k_p and it shows the same behaviour for all other flow variables.

The expressions for the variations in the flow variables given in Eqs. (26–29) within the shock transition region with the distance (r) for different values of μ and k_p at fixed values of $M=2$, $G=10$, $\gamma = 1.4$, $\beta = 1$, $p_0 = 0.9$ bar, $\rho_0 = 1.20$ kg m^3 are shown in Fig. 3. It is observed that the spreading of the particle velocity (η), and pressure distribution (p/p_0) are distinguishable in both the regions of the stream. For the case of temperature (T/T_0) and change-in-entropy distribution ($\Delta s/R_i$), the variations are distinguishable for the downstream region while these become indistinguishable for the upstream region. We also notice that the entropy distribution ($\Delta s/R_i$) shows large inflection before it becomes indistinguishable towards the upstream side.

We are getting two different types of structure lines in Fig. 3. In Fig. 3b, c, i.e. in the T/T_0, p/p_0 distributions, the distribution shows large spreading at $\mu = 15 \times 10^{-6}$ Pa s and $k_p = 0$. It can be seen that the order of spreading at fixed value of k_p and for different values of μ ($15 \times 10^{-6} \le \mu \le 20 \times 10^{-6}$ Pa s) is same before becoming indistinguishable in the downstream side. On the other hand, in Fig. 3a, d, the spreading is large at $\mu = 15 \times 10^{-6}$ Pa s, and $k_p = 0$, and the order of spreading for fixed value of μ and different value of k_p ($0 \le k_p \le 0.3$) is same. This sequence remains the same for each value of μ corresponding to k_p in Fig. 3b, c and a, d, respectively.

The expressions for the variations in the flow variables within the shock transition region with the distance (r) for different values of M and k_p at a fixed value of $G=10$, $\mu = 15.0 \times 10^{-6}$ Pa s, $\gamma = 1.4$, $\beta = 1$, $p_0 = 0.9$ bar, $\rho_0 = 1.20$ kg m^3 are shown in Fig. 4. It can be observed from Fig. 4, that all the flow variables are distinguishable towards the downstream side, while indistinguishable in the direction of the upstream side. For the case of entropy distribution ($\Delta s/R_i$), the variation is distinguishable towards the downstream side, whereas it shows much inflection before being identical towards the upstream side.

It can also be noticed from Fig. 4a, c for the distribution of η and p/p_0 given a fixed value of $M=2$ and $k_p = 0.3$, the spreading is large. Also, with increasing k_p while keeping M constant, the spreading of the flow variables increase. The pattern of the distribution is similar for each decreasing value of M from 2 to 1.1.

Coming to the case of T/T_0 and $\Delta s/R_i$, the spreading of the flow variables is large at fixed value of $M=2$, $k_p = 0$, and with increasing k_p, taking M constant, the spreading of the flow variables decreases (see Fig. 3b, c). From the above observations, we can conclude that, for a two=phase dusty medium, as the strength of shock increases, the thickness of the shock-front decreases.

6 Conclusions

In the present study, one-dimensional exact solutions of the flow variables (η, T/T_0, p/p_0 *and* $\Delta s/R_i$) in two-phase gas–solid particle flow are obtained using Navier–Stokes equations. The thickness of the shock-front within the shock transition region has been explored. Obtained results show that the dust loading parameters as well as Mach numbers, coefficient of viscosity have an impressive impact on the thickness of the shock wave-front. This work of shock waves in a two-phase flow medium provides a good introduction to the real-gas effect. From tables and figures, one may draw following conclusions:

1. The thickness of the shock-front increases as we go from dust-free ($k_p = 0$) to dusty gaseous medium ($k_p = 0.1$) for different values of shock strength while it decreases in the case of $M=1.1$. On further increasing the value of k_p from 0.1 to 0.3, the thickness of the shock-front increases. Note that the obtained results are the same for all values of μ in the range

$15 \times 10^{-6} \leq \mu \leq 20 \times 10^{-6}$ Pa s (see Table 1 and Figs. 1, 3, 4).

2. Further, the thickness of shock-front increases with increasing dust loading parameter G, and follows the same behaviour with the flow variables $\eta,\ T/T_0,\ p/p_0$ *and* $\Delta s/R_i$ (see Table 2, Fig. 2). However, in comparison with the parameter k_p, the thickness is less affected by G.
3. On increasing the value of μ, the thickness of shock-front increases in both dust-free ($k_p = 0$) and dusty gaseous ($k_p \neq 0$) media. It is also notable that for each value of μ, the thickness increases with increasing k_p. Interestingly, the above effects are more prominent as k_p lies in the range $0 \leq k_p \leq 0.4$ and for all possible values of μ (see Table 1, Fig. 3)
4. The thickness of the shock-front decreases with increasing M and remains the same for k_p varying from 0 to 0.4. In this range, it is also remarkable that the thickness variation is the same for each value of μ (see Table 1, Fig. 4)

Thus, the present study describes an investigation into the nature of shock waves in a two-phase gas–solid particle mixture. We found that the obtained results give more precise and simpler concepts about the inner structure of the shock wave-front in a dusty gaseous medium. This study on the structure of shock waves in dusty gases will provide a path forward in environmental research, in geophysics as well as in space science research.

Relevance of research The present study is of interest to the fluid dynamicists and scientists working on the shock waves in viscous media. The findings obtained here are important for the various industrial and mechanical engineering processes where two-phase gas–particle viscous fluids play significant roles. The results are useful in investigating the effects of viscosity on blood circulation, cardiovascular events, crude oil transportation, etc.

Funding The authors have not received any type of funding whether governmental or non-governmental for this scholarly work.

Data Availability The data generated or analysed during this study are included in this published article.

Code Availability Not applicable.

Declarations

Conflict of interest The authors declare that there is no conflict of interest regarding the publication of this research paper.

References

1. Rudinger G (1980) Fundamentals of gas–particle flow. Elsevier, Amsterdam
2. Kriebel R (1964) Analysis of normal shock waves in particle laden gas. J Basic Eng 86:655–664
3. Marble FE (1963) Dynamics of a gas containing small solid particles Combustion and propulsion. Pergamon Press, Oxford
4. Marble FE (1970) Dynamics of dusty gases. Annu Rev Fluid Mech 2:397–446
5. Outa E, Tajima K, Morii H (1976) Experiments and analyses on the shock waves propagating through a gas–particle mixture. Bull JSME 19:384–394
6. Igra O, Ben-Dor G (1988) Dusty shock gases. Appl Mech Rev 41:379–437
7. Kraiko AN, Nigmatulin RI, Starkov VK, Sterlin LE (1972) Mechanics of multiphase media. In: Advances in science and technology hydromechanics. VINITI, Moscow
8. Ivandaev AI, Kutushev AG, Nigmatulin RI (1981) Gasdynamics of multiphase media. Shock and detonation waves in gas-particle mixtures. In: Advances in science and technology. Mechanics of liquids and gases. VINITI, Moscow
9. Carrier GF (1958) Shock waves in a dusty gas. J Fluid Mech 4:376–382
10. Rudinger G (1965) Some effects of finite particle volume on the dynamics of gas–particle mixture. AIAA J 3:1217–1222
11. Ben-Dor G (1996) Dusty shock waves: an update. Appl Mech Rev 49:141–146
12. Pai SI (1977) Two-phase flow vieweg tracts in pure and applied physics. Vieweg Verlag, Braunschweig
13. Pai SI, Menon S, Fan ZQ (1980) Similarity solution of a strong shock wave propagation in a mixture of a gas and dust particles. Int J Eng Sci 18:1365–1373
14. Higashino F, Suzuki T (1980) The effects of particles on blast wave in dusty gas. Z Naturforsch A 35:1330–1336
15. Gintrand A, Sanz J, Bouquet S et al (2020) Self similar dynamics of radiative blast waves. Phys Fluids 32:16105
16. Gretler W, Regenfelder R (2005) Strong shock waves generated by a piston moving in a dust-laden gas under isothermal conditions. J Eng Math 52:321–336
17. Miura H, Glass II (1985) Development of the flow induced by a piston moving impulsively in a dusty gas. Proc Roy Soc Lond A 397:295–309
18. Miura H (1990) Decay of shock waves in a dusty-gas tube. Fluid Dyn Res 6:251–259
19. Gupta P, Chaturvedi RK, Singh LP (2020) Interaction of waves in one-dimensional dusty gas flow. Z Naturforsch A 76:201–208
20. Anand RK (2014) Shock jump relations for a dusty gas atmosphere. Astrophys Space Sci 349:181–195
21. Nath G (2010) Propagation of a strong cylindrical shock wave in a rotational axisymmetric dusty gas with exponentially varying density. Res Astron Astrophys 10:445–460
22. Arora R, Chauhan A (2020) Self-similar solutions of cylindrical shock wave in a dusty gas. Indian J Phys 94:665–673
23. Anand RK (2018) On the strong spherical shock waves in a two-phase gas-particle medium. J Appl Comput Math 4:49
24. Hamad H (1998) Behavior of entropy across shock waves in dusty gases. Z Angew Math Phys 49:827–837
25. Hamad H (1999) On the structure of shock waves in dusty gases. Indian J Pure Appl Math 30:485–490
26. Robben F, Talbot L (1996) Measurement of shock wave thickness by the electron beam fluorescence method. Phys Fluids 9:633–643
27. Elizarova TG, Shirokov IA, Montero S (2005) Shock wave structure for argon, helium, and nitrogen. Rarefied Gas Dynamics. In: AIP conference proceedings, vol 762, pp 1253–1258
28. Shoev GV, Timokhin MY, Bondar YA (2020) On the total enthalpy behavior inside a shock wave. Phys Fluids 32:041703
29. Bisi M, Groppi M, Martalo G (2020) On the shock thickness for a binary gas mixture. Ricerche mat 70:51–66

30. Wei T, Hargather MJ (2021) A new blast wave scaling. Shock Waves 31:231–238
31. Ling Y, Balachandar S (2018) Simulation and scaling analysis of a spherical particle laden blast wave. Shock Waves 28:545–558
32. Elizarova TG, Shirokov IA, Montero S (2007) Numerical simulation of shock wave structure in nitrogen. Phys Fluids 19:5–9
33. Steven B, Colonius T (2020) Enhancement of shock-capturing methods via machine learning. Theor Comput Fluid Dyn 34:483–496
34. Berselli LC, Cerminara M, Iliescu T (2015) Disperse Two-phase flows with applications to geophysical problems. Pure Appl Geophys 172:181–196
35. Drake RP, Keiter PA, Kuranz CC et al (2016) Study of shock waves and related phenomena motivated by astrophysics. J Phys Conf Ser 688:012016
36. Takayama K, Ohtani K (2005) Applications of shock wave research to medicine. Trans Model Simul 41:653–661
37. Zapryagaev V, Kiselev N, Gubanov D (2018) Shock wave structure of supersonic jet flows. Aerospace 5:60
38. Ligrani PM, McNabb ES, Collopy H et al (2020) Recent investigations of shock wave effects and interactions. Aerodynamics 2:4
39. Masser TO, Wohlbier JG, Lowrie RB (2011) Shock wave structure for a fully ionized plasma. Shock Waves 21:367–381
40. Golshan AN (2018) Investigation of cylindrical shock waves in dusty plasma. Indian J Phys 92:1643–1650
41. Shreekhar, Akhil M, Ram S et al (2018) Study of the effects of shock waves on nano fluids. IOP Conf Ser Mater Sci Eng 310:012105
42. Cuenca E, Ducousso M, Rondepierre A et al (2020) Propagation of laser-generated shock waves in metals: 3D axisymmetric simulations compared to experiments. J Appl Phys 128:244903
43. Clauer AH, Holbrook JH, Fairand BP (1981) Shock waves and high strain rate phenomena in metals. Plenum Publishing Corporation, New York
44. Anand RK (2020) On the shock dynamics of weak converging shock waves in solid materials. Ricerche mat. https://doi.org/10.1007/s11587-020-00545-1
45. Anand RK, Yadav HC (2016) The effects of viscosity on the structure of shock waves in non-ideal gas. Acta Phys Pol A 129:28–34